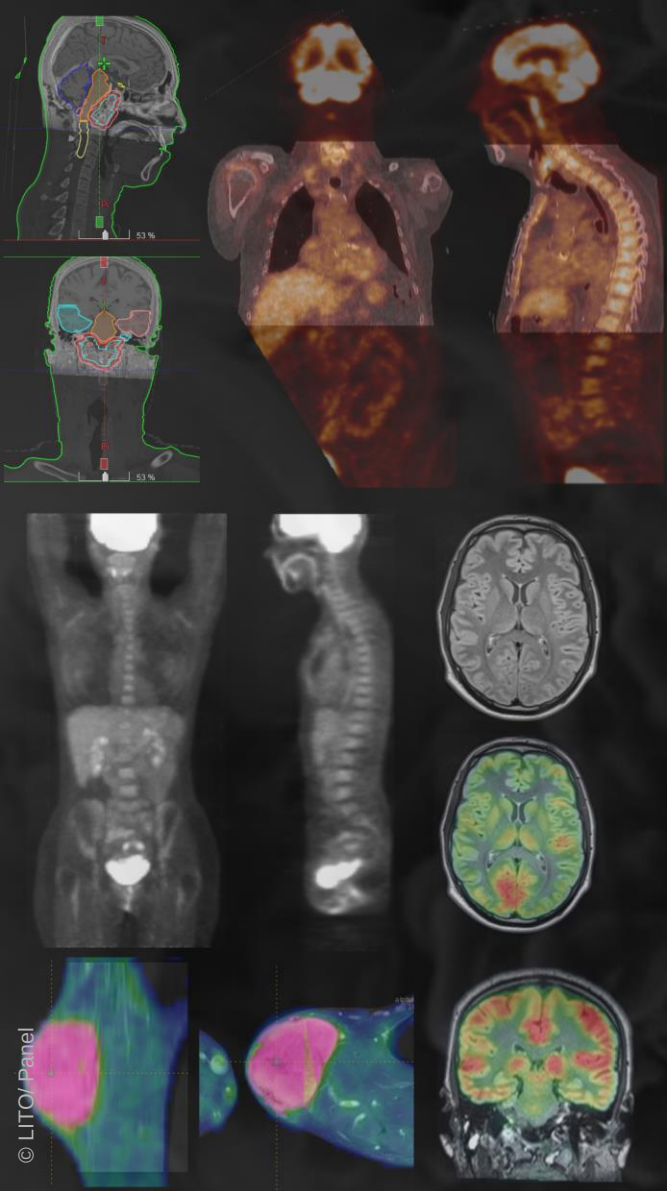

LITO

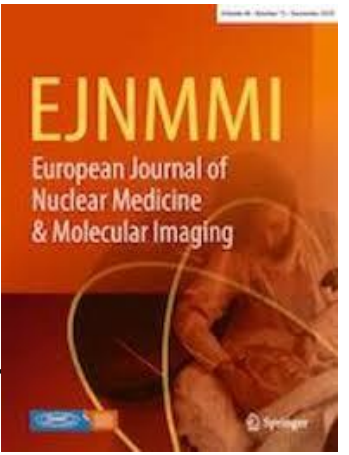

European Journal of Nuclear Medicine and Molecular Imaging
https://doi.org/10.1007/s00259-019-04625-9

ORIGINAL ARTICLE

Radiomics of ^{18}F-FDG PET/CT images predicts clinical benefit of advanced NSCLC patients to checkpoint blockade immunotherapy

Wei Mu[1] · Ilke Tunali[1] · Jhanelle E. Gray[2] · Jin Qi[1] · Matthew B. Schabath[2,3] · Robert J. Gillies[1]

[1] Department of Cancer Physiology, H. Lee Moffitt Cancer Center and Research Institute, 12902 Magnolia Drive, Tampa, FL 33612, USA

[2] Department of Thoracic Oncology, H. Lee Moffitt Cancer Center and Research Institute, Tampa, FL, USA

[3] Department of Cancer Epidemiology, H. Lee Moffitt Cancer Center and Research Institute, Tampa, FL, USA

Published online: 05 December 2019

04/06/2020

Contexte

- Thérapies anti-PD/PD-L1 ont un bénéfice clinique seulement pour un sous-groupe de patients (~15-20%) → nécessité d'identifier des biomarqueurs robustes

- Durable Clinical Benefit (DCB)/ No Durable Benefit (NDB) : PFS < ou > à 6 mois

Objectif de l'étude :

déterminer si l'analyse radiomique des images TEP/TDM avant traitement, seule ou en combinaison avec des facteurs cliniques, peut permettre de prédire la réponse à l'immunothérapie, PFS et OS

→ Construction d'un nomogramme en combinant une signature multiparamétrique radiomique (**mpRS**) avec des données cliniques

Contexte

- Aujourd'hui : évaluation du statut PD-L1 des tumeurs par immunohistologie mais possible biais d'échantillonnage

22.9 to 61.4% regardless of PD-L1 status [11]. Additionally, intra-tumor heterogeneity of PD-L1 staining across biopsies is prevalent, leading to sampling bias [12]. There have been

- Les tumeurs PD-L1 négatives peuvent bénéficier d'une thérapie anti-PDL1

[8, 9]. However, patients with PD-L1-negative tumors can still benefit from anti-PD-(L)1 therapies [6, 10]. A recent study showed that a combination of pembrolizumab and chemotherapy achieved objective radiographic response rates, ORRs, of 22.9 to 61.4% regardless of PD-L1 status [11]. Additionally,

→ Intérêt limité à quantifier le statut PD-L1 (?), il faut peut-être plutôt chercher à prédire la réponse

Contexte

Avantages de la Radiomique :

- Technique non-invasive
- Suivi longitudinal possible
- Basée sur des images déjà acquises pendant le parcours de soin
- Hétérogénéité de la tumeur en entier et des métastases
  (sans biais d'échantillonnage) … mais avec une résolution spatiale plus limitée

Workflow

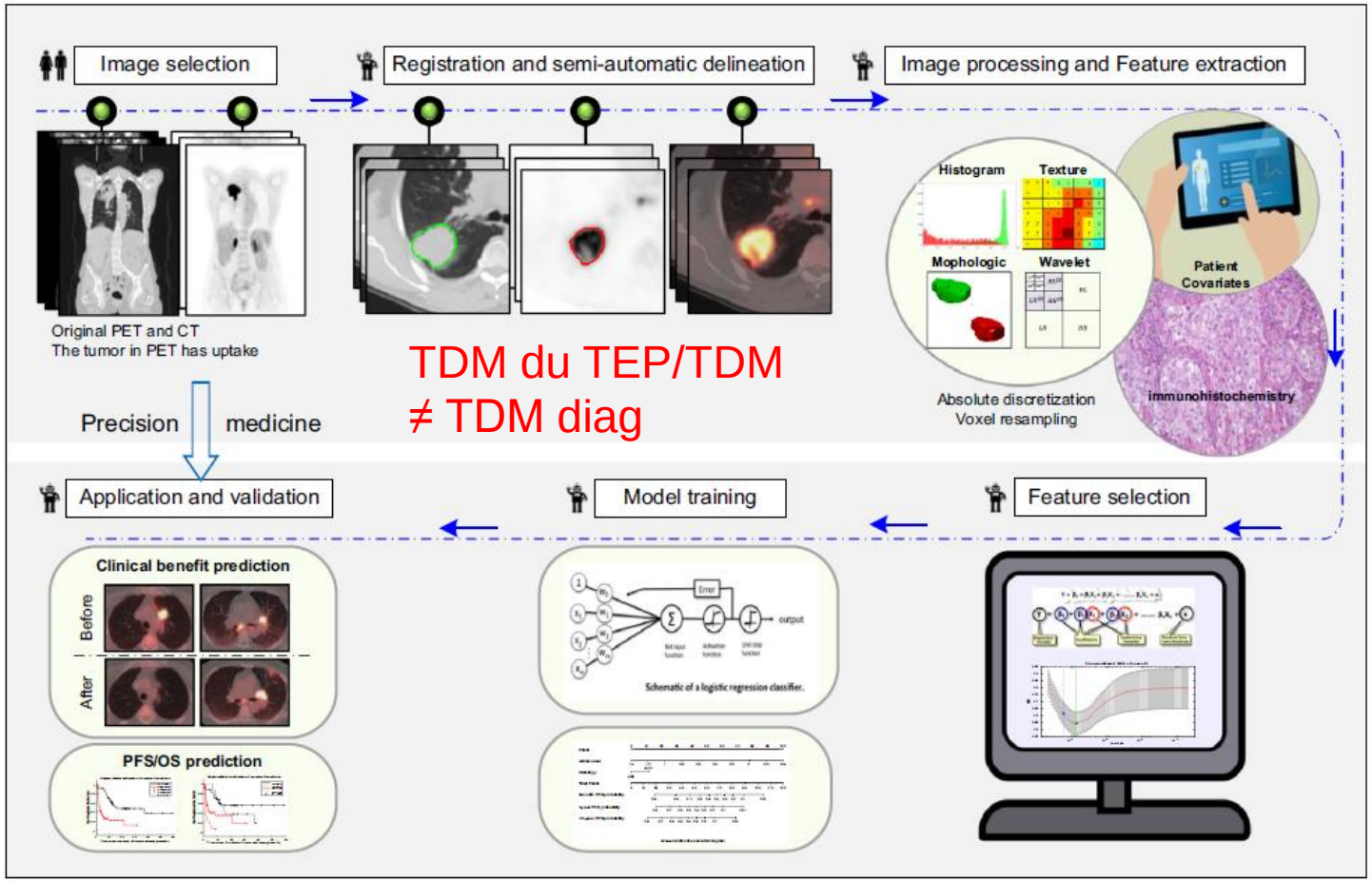
Image selection
Registration and semi-automatic delineation
Image processing and Feature extraction
Original PET and CT
The tumor in PET has uptake
Histogram
Texture
Mophologic
Wavelet
Patient Covariates
Absolute discretization
Voxel resampling
immunohistochemistry
TDM du TEP/TDM
≠ TDM diag
Precision medicine
Application and validation
Model training
Feature selection
Clinical benefit prediction
Before
After
PFS/OS prediction
Schematic of a logistic regression classifier.

Patients

Fig. 2 Inclusion and exclusion diagram. The training cohort comprised clinical data, and the corresponding imaging data of the retrospective patients were used to train the radiomics signature, the DCB, and the PFS and OS nomogram models, which were further validated using the test cohort of the retrospective patients and the prospective cohort enrolled according to the same inclusion and exclusion criteria

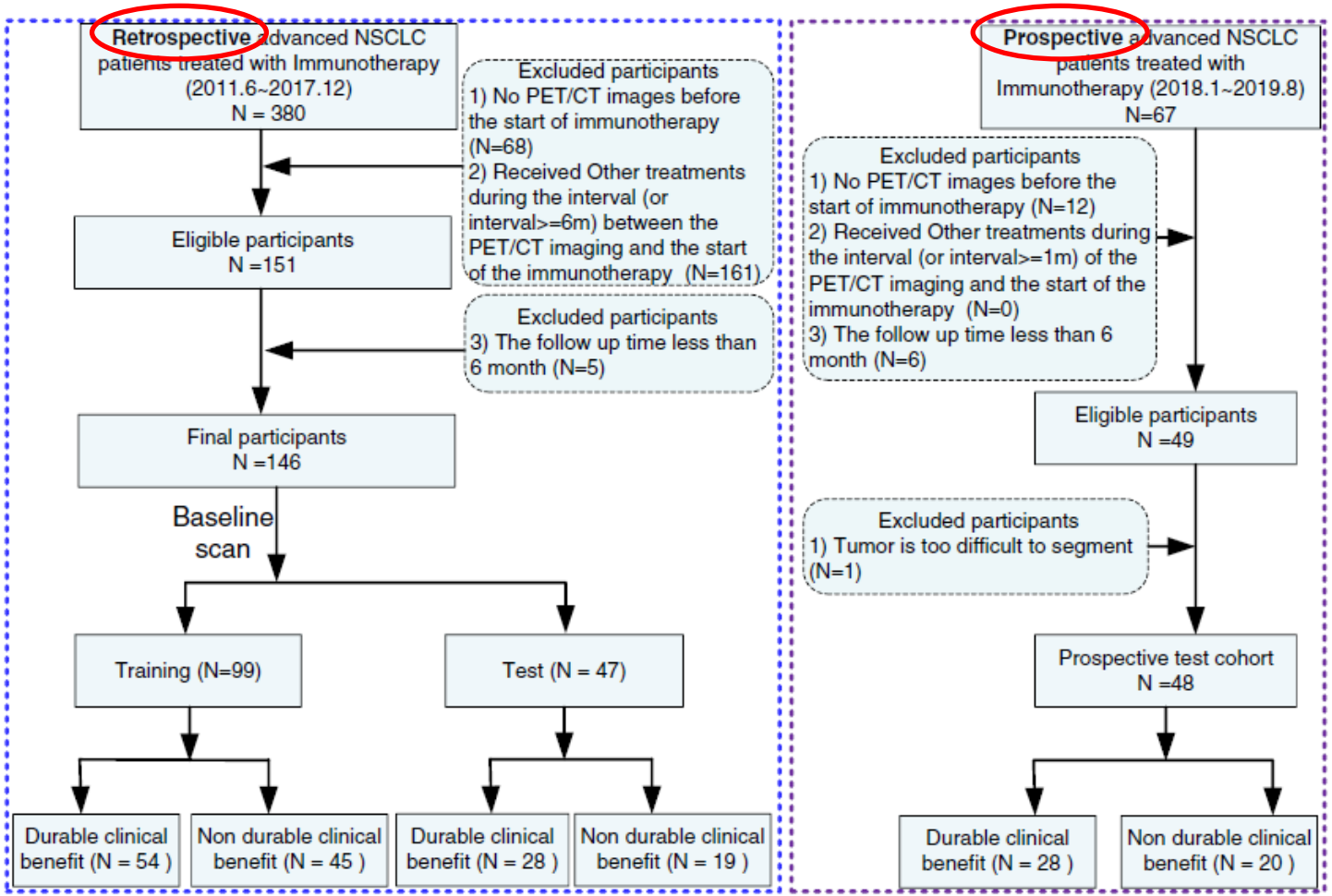

Acquisition TEP/TDM

PET/CT imaging

^{18}F-FDG PET/CT imaging was performed as standard diagnostic work-up before treatment with immunotherapy. Details of the retrospective PET/CT images obtained from 9 different scanners and the prospective PET/CT images obtained from 2 different scanners are shown in Supplemental Methods S1. Heterogeneity in scanner parameters was deliberately chosen to ensure generalizability of the derived predictive models. All PET images were converted into SUV units by normalizing the activity concentration to the dosage of ^{18}F-FDG injected and the patient body weight after decay correction. Further, all the PET and CT images were resampled to $1 \times 1 \times 1$ mm^3 voxels using 3-dimensional Lagrange interpolating polynomials.

→ 9 systèmes TEP/CT sans correction/harmonisation (données de « vie réelle »)

Création d'une image de fusion TEP/TDM

who was blinded to the outcome label. After spatial registration using a rigid transformation by maximizing the dice similarity coefficients on the condition that the maximal axial cross-sections of the nodules were aligned, Kullback–Leibler divergence (KLD) images were generated from the fused PET and CT images on a voxel-wise basis using KLD criteria [21].

Images de divergence Kullback-Leiber

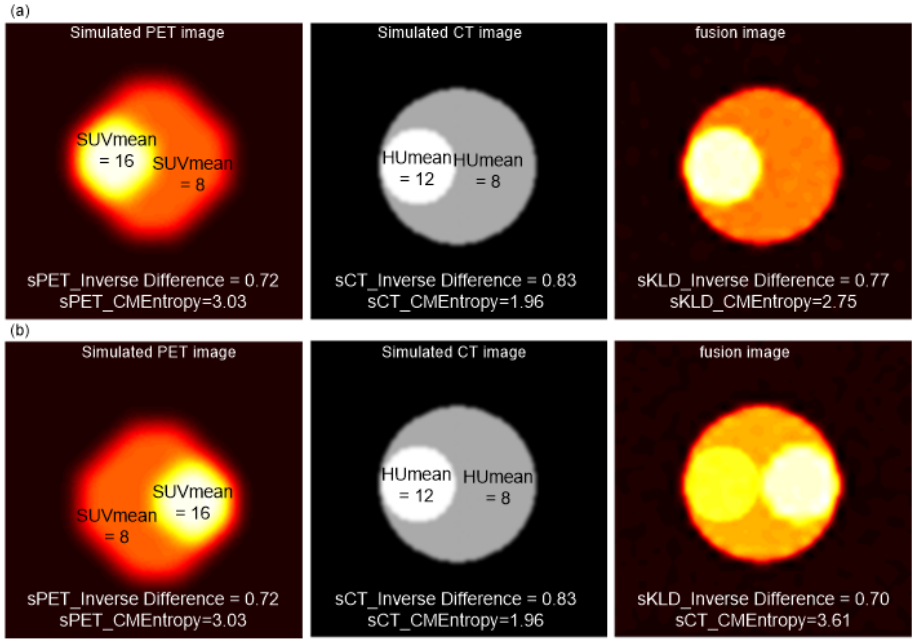

Fig S3. Two different digital simulated phantoms were constructed as a and b. In order to show the importance of the KLD features, a and b were kept to have the same heterogeneity distribution. Entropy and Inverse Difference calculated from 3D co-occurrence matrix were used to measure the heterogeneity and the homogeneity of the phantoms. From the simulated PET images (the first column) and simulated CT images (the second column), the two phantoms have the same heterogeneity and homogeneity distribution. But from the fusion images (the third column), the two phantoms could be identified based on different heterogeneity and homogeneity, which means the KLD features could reflect the relative different positional relationship of the heterogeneity.

hereafter. The fusion images were calculated through the equation:

$$I_{FUSE} = I_{PETnorm} + \alpha I_{CTnorm}, \tag{4.1}$$

where $I_{PETnorm}$ and I_{CTnorm} are the normalized PET and CT pixel-wise image data with the following scheme to keep the negative values in CT images:

$$I_{Xnorm} = \frac{I_X}{\max(I_X)} (X \text{ represents PET or CT}), \tag{4.2}$$

α was selected based on the following improved minimum KLD criterion:

$$\alpha = \arg\min_{\alpha \in [0.4,1]} \left(\sum_{i=0}^{L} p_{PET}(i) \log_2 \left| \frac{p_{PET}(i)}{p_{FUSE}(i)} \right| + \sum_{i=0}^{L} p_{CT}(i) \log_2 \left| \frac{p_{CT}(i)}{p_{FUSE}(i)} \right| \right), \tag{4.3}$$

where p_{PET} , p_{CT} and p_{FUSE} are the normalized histograms of the PET, CT, and fusion images, respectively. L is the number of bins and was set to 128 in this study. After training, α was set to 0.6 in

→ Création d'une image de fusion pour mutualiser l'information des SUVs et des UH

Segmentation/Analyse radiomique

The primary lung tumors of PET and CT images were semi-automatically segmented with an improved level-set method based on gradient fields [19] and were further reviewed and corrected by a radiologist with 16 years of experience (JQ)

Seven hundred ninety features including PET features, CT features, and KLD features were then extracted from these segmented tumors and scaled into the range [0 1] with unity-based normalization, as shown in Supplemental Methods S2-

364 features en TEP
+ 364 features en TDM
+ 62 features pour KLD
= 790

Group1: Three dimensional PET imaging features. A total of 364 3D imaging features of the tumor from PET images, including 209 features (including 62 textural features, 48 statistical features, 42 morphological features, and 57 diagnostic features) described in ref (S1), and an additional 125 Laws features and 30 wavelet features (Supplemental Methods S 3) were calculated.

Group II: Three dimensional CT imaging features. Similar to PET imaging features, the same set of 364 3D imaging features of the tumor from CT images was also extracted.

Group III: Three dimensional KLD imaging features. Fusion imaging plays an important role in clinic, since it can provide the location and boundary information from CT images in addition to the metabolic information from PET images. This is currently processed mentally by the nuclear medicine physician or oncologist. To perform quantitative fusion, we constructed fusion images based on improved minimum Kullback–Leibler Divergence (KLD) criteria (Supplemental Methods S4), named KLD images hereafter. From this KLD image, 62 textural of the 364 features were calculated.

1ère sélection des index

Supplemental Methods S5: Internal stability

Through bootstrapping of training data (100 times), only the features with the lower 95% confidence bound of areas under receiver operating characteristics curves (AUC) larger than 0.5 (or the upper 95% confidence bound smaller than 0.5) were regarded stable enough for the following analysis, and the average AUC was regarded as the internal stability for each feature.

(// avec le tri par les p-values du test de Wilcoxon)

Of the original 790 extracted features, 324 remained after filtering for internal stability.

Analyse non-supervisée

Unsupervised clustering revealed 3 clusters of patients with similar radiomics expression patterns (Fig. 3a), which were significantly associated with histology ($P = 0.008$, $\chi 2$ test) and response ($P = 0.028$, $\chi 2$ test). The prospective patients further showed similar radiomics expression patterns and validated this association of these radiomics feature patterns with histology ($P = 0.041$, $\chi 2$ test) and response ($P = 0.085$, $\chi 2$ test) (Fig. 3b).

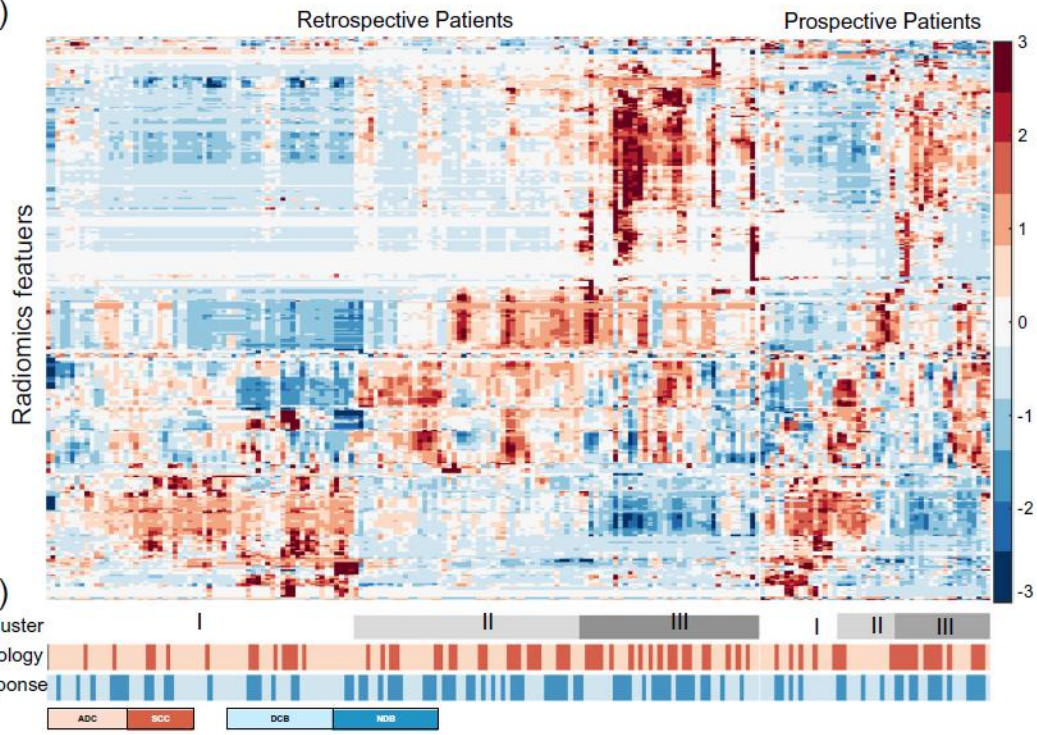

→ 3 clusters établis sur la cohorte rétrospective puis validés sur la cohorte prospective

→ Lien avec l'histologie et la réponse

Sélection par le coefficient de corrélation de Pearson

Specifically, in order to reduce the dimension of the input vector, a prioritized list of features based on their prognostic power and redundancies were firstly selected. In order to reduce redundancy, the selected features were divided into different groups to ensure the absolute value Pearson correlation coefficient (denoted by $|r|$) between any pairs of features in the same group was greater than 0.6 and $|r|$ between any pairs of features from any two different groups was smaller than 0.6. Then the features with the largest internal stability in each correlated group were selected to represent that group in subsequent analyses.

Pearson grouping was used to eliminate redundant features, resulting in 21 uncorrelated features (10 PET features, 4 CT features, and 7 KLD features). These were

790 features → 324 features → 21 features

Construction des signatures radiomiques

Supplemental Methods S6. Improved LASSO method

The response status of the patients was estimated with the imaging features with the following model:

$$y = (2-h)\sum_{i=1}^{p}\beta_{1i}x_i + (h-1)\sum_{j=1}^{p}\beta_{2j}x_j + \alpha_1 h + \alpha_0, \quad (6.1)$$

where y was the response status of the patients; p was the number of features; x_i (i = 1, 2, ..., n) was the independent parameter; β_{1i} (i = 1, 2, ..., n) was the coefficient of ADC; β_{2i} (i = 1, 2, ..., n) was the coefficient of SCC; α (i = 0,1) was the coefficient of histology; h was the histology of the patient (ADC: h=1; SCC: h=2). By forcing many parameters to zero, feature selection can be performed. The aim was to minimize the following cost function:

$$\min_{\alpha_0,\alpha_1,\beta_1,\beta_2}\left(\frac{1}{2N}\sum_{i=1}^{N}\left(y_i-\alpha_0-\alpha_1 h-(2-h)x_i^T\beta_1-(h-1)x_i^T\beta_2\right)^2+\lambda_1\sum_{j=1}^{p}\left|\beta_{1j}\right|+\lambda_2\sum_{j=1}^{p}\left|\beta_{2j}\right|\right) \quad (6.2)$$

where y_i was the response status of the ith patient; N was the number of patients; λ_1 and λ_2 were tuning parameters, which were selected using 10-fold cross validation via minimum criteria. A radiomics signature was calculated for each patient via a linear combination of selected features that were weighted by the corresponding coefficients.

→ Signature radiomique avec prise en compte du sous-type histologique

Signature radiomique

There were significant differences in the four radiomics signature scores between DCB and NDB patients in the training cohort (PETRS: $P < 0.001$; CTRS: $P = 0.020$; PETCTRS: $P < 0.001$; mpRS: $P < 0.001$). Except for the CTRS, the other three radiomics signatures had significant differences between DCB and NDB patients in the retrospective (PETRS: $P = 0.006$; PETCTRS: $P = 0.003$; mpRS: $P < 0.001$) and prospective (PETRS: $P = 0.019$; PETCTRS: $P = 0.009$; mpRS: $P < 0.001$) test cohorts.

different radiomics signatures were obtained: PET radiomics signature (i.e., PETRS) obtained from Group I, CT radiomics signature (i.e., CTRS) obtained from Group II, PET+CT radiomics signature (i.e., PETCTRS) obtained from Groups I and II, and the multimodality fused radiomics signature (i.e., mpRS) obtained from combining all groups I to III.

Et les résultats uniquement avec l'image de fusion svp ???

TEP TDM TEP+TDM TEP+TDM+Fusion

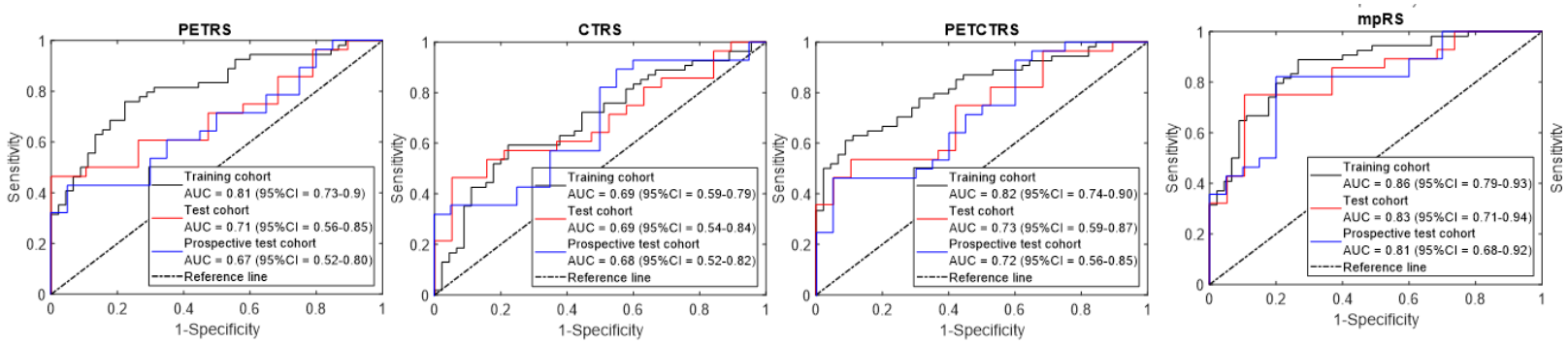

Signatures radiomiques : NRI

Fig. S4). Compared with PET+CT features, the inclusion of the KLD features yielded a total net reclassification improvement (NRI) of 0.50 (95%CI 0.11–0.88, $P = 0.011$), 0.55 (95%CI −0.012–1.11, $P = 0.055$), and 0.94 (95%CI 0.44–1.45, $P < 0.001$) in the training, test, and prospective test cohorts, respectively, which showed significantly improved classification accuracy for response prediction. Therefore, only mpRS was used for the subsequent analyses.

Table S1. Performance of different radiomics signatures and different models in DCB prediction

	AUC(95% CI)	ACC(95% CI)	SEN (95% CI)	SPEC(95% CI)	AIC	p
PETRS						
Training	0.81(0.73-0.90)	76.77(67.67-83.84)	0.76(0.61-0.85)	0.78(0.64-0.89)	109.62	0.01
Test	0.71(0.56-0.85)	63.83(51.06-78.72)	0.61(0.43-0.79)	0.68(0.47-0.89)	61.49	0.03
Prospective	0.67(0.52-0.80)	64.58(52.08-72.92)	0.43(0.21-0.57)	0.95(0.50-1.00)	64.56	0.12
CTRS						
Training	0.69(0.59-0.79)	67.68(56.57-75.76)	0.59(0.44-0.72)	0.78(0.66-0.89)	134.47	0.10
Test	0.69(0.54-0.84)	63.83(48.94-76.60)	0.57(0.38-0.75)	0.74(0.53-0.95)	63.67	0.10
Prospective	0.68(0.52-0.82)	70.83(58.33-81.05)	0.89(0.71-0.96)	0.45(0.25-0.65)	63.69	0.10
PETCTRS						
Training	0.82(0.74-0.9)	74.75(65.66-81.29)	0.61(0.46-0.72)	0.91(0.82-0.98)	106.78	0.67
Test	0.73(0.59-0.87)	65.96(55.32-78.72)	0.50(0.29-0.64)	0.89(0.84-1)	58.97	0.13
Prospective	0.72(0.56-0.85)	66.67(52.08-77.08)	0.46(0.25-0.61)	0.95(0.85-1)	64.95	0.050
mpRS						
Training	0.86(0.79-0.93)	81.82(72.73-87.88)	0.89(0.78-0.95)	0.73(0.60-0.87)	95.03	0.61
Test	0.83(0.71-0.94)	76.60(63.83-88.24)	0.75(0.57-0.89)	0.79(0.58-0.95)	51.87	0.16
Prospective	0.81(0.68-0.92)	81.25(70.83-91.67)	0.82(0.68-0.96)	0.80(0.60-0.95)	53.85	0.34

→ Les index mesurés sur l'image de fusion apportent des informations différentes/complémentaires

Rappel : Net Reclassification Improvement (NRI)

This measure has been proposed as an alternative to the area of the the receiver operating characteristic curve.[4][19] This method allows calculating a 'reclassification index' or 'reclassification rate', or 'net reclassification improvement' (NRI).[19]

$$\text{NRI} = \text{ sum of:}$$

$$\frac{\text{events reclassified higher} - \text{events reclassified lower}}{\text{events}}$$

and

$$\frac{\text{nonevents reclassified lower} - \text{nonevents reclassified higher}}{\text{nonevents}}$$

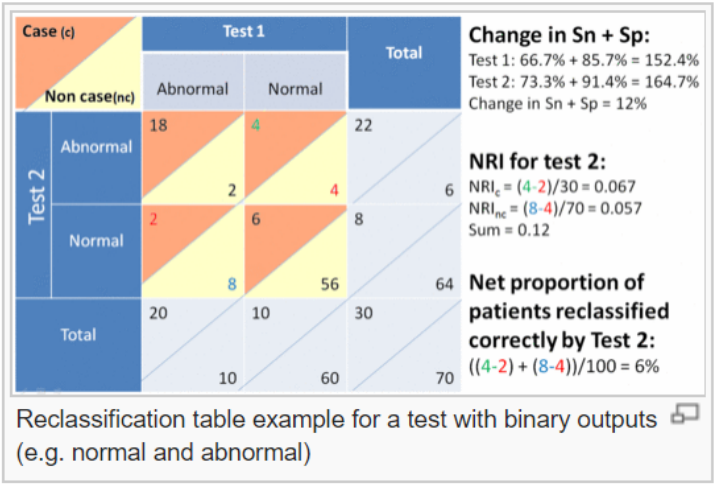

Reclassification table example for a test with binary outputs (e.g. normal and abnormal)

The NRI is analogous to Youden's *J* index and the Gain in Certainty which are both functions of the sum of the sensitivity and specificity. In the special case of two diagnostic tests that have binary results (e.g. normal and abnormal), the NRI is the same the Gain in Certainty of the first test minus the Gain in Certainty of the second test, or alternatively stated, the change in the sum of the sensitivity and specificity:

$$\text{NRI}_{\text{for tests with binary outcomes}} = (\text{Sensitivity} + \text{Specificity})_{\text{Second test}} - (\text{Sensitivity} + \text{Specificity})_{\text{First test}}$$

// gain en Youden

Rappel : Net Reclassification Improvement (NRI)

30 cas / 70 non-cas

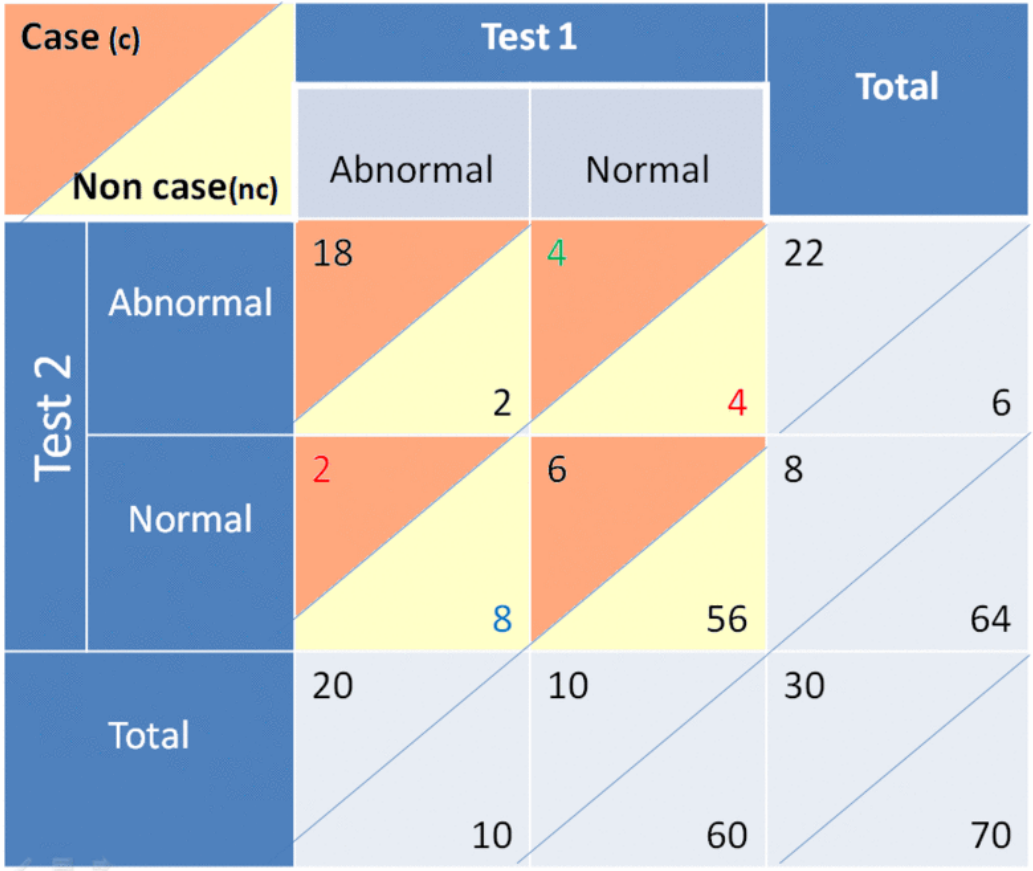

Case (c) / Non case (nc)		Test 1: Abnormal	Test 1: Normal	Total
Test 2	Abnormal	18 / 2	4 / 4	22 / 6
Test 2	Normal	2 / 8	6 / 56	8 / 64
Total		20 / 10	10 / 60	30 / 70

Change in Sn + Sp:

Test 1: 66.7% + 85.7% = 152.4%

Test 2: 73.3% + 91.4% = 164.7%

Change in Sn + Sp = 12%

NRI for test 2:

$NRI_c = (4-2)/30 = 0.067$

$NRI_{nc} = (8-4)/70 = 0.057$

Sum = 0.12

Net proportion of patients reclassified correctly by Test 2:

((4-2) + (8-4))/100 = 6%

Signatures radiomiques : NRI

Fig. S4). Compared with PET+CT features, the inclusion of the KLD features yielded a total net reclassification improvement (NRI) of 0.50 (95%CI 0.11–0.88, $P = 0.011$), 0.55 (95%CI −0.012–1.11, $P = 0.055$), and 0.94 (95%CI 0.44–1.45, $P < 0.001$) in the training, test, and prospective test cohorts, respectively, which showed significantly improved classification accuracy for response prediction. Therefore, only mpRS was used for the subsequent analyses.

Table S1. Performance of different radiomics signatures and different models in DCB prediction

	AUC(95% CI)	ACC(95% CI)	SEN (95% CI)	SPEC(95% CI)	AIC	p
PETRS						
Training	0.81(0.73-0.90)	76.77(67.67-83.84)	0.76(0.61-0.85)	0.78(0.64-0.89)	109.62	0.01
Test	0.71(0.56-0.85)	63.83(51.06-78.72)	0.61(0.43-0.79)	0.68(0.47-0.89)	61.49	0.03
Prospective	0.67(0.52-0.80)	64.58(52.08-72.92)	0.43(0.21-0.57)	0.95(0.50-1.00)	64.56	0.12
CTRS						
Training	0.69(0.59-0.79)	67.68(56.57-75.76)	0.59(0.44-0.72)	0.78(0.66-0.89)	134.47	0.10
Test	0.69(0.54-0.84)	63.83(48.94-76.60)	0.57(0.38-0.75)	0.74(0.53-0.95)	63.67	0.10
Prospective	0.68(0.52-0.82)	70.83(58.33-81.05)	0.89(0.71-0.96)	0.45(0.25-0.65)	63.69	0.10
PETCTRS						
Training	0.82(0.74-0.9)	74.75(65.66-81.29)	0.61(0.46-0.72)	0.91(0.82-0.98)	106.78	0.67
Test	0.73(0.59-0.87)	65.96(55.32-78.72)	0.50(0.29-0.64)	0.89(0.84-1)	58.97	0.13
Prospective	0.72(0.56-0.85)	66.67(52.08-77.08)	0.46(0.25-0.61)	0.95(0.85-1)	64.95	0.050
mpRS						
Training	0.86(0.79-0.93)	81.82(72.73-87.88)	0.89(0.78-0.95)	0.73(0.60-0.87)	95.03	0.61
Test	0.83(0.71-0.94)	76.60(63.83-88.24)	0.75(0.57-0.89)	0.79(0.58-0.95)	51.87	0.16
Prospective	0.81(0.68-0.92)	81.25(70.83-91.67)	0.82(0.68-0.96)	0.80(0.60-0.95)	53.85	0.34

$$\mathrm{NRI}_{\text{for tests with binary outcomes}} = (\text{Sensitivity} + \text{Specificity})_{\text{Second test}} - (\text{Sensitivity} + \text{Specificity})_{\text{First test}}$$

NRI = (0.89+0.73) - (0.61+0.91)

= 0.10

≠ 0.50

Impact des paramètres d'acquisition et reconstruction

Box plots and ANOVA analyses of each of the radiomics signatures are shown in Supplemental Fig. S5, which illustrates that these signatures are stable across 9 different equipment manufacturers ($P > 0.05$), with mpRS being the most stable signature with the fewest outliers.

→ Pas de correction à appliquer car la signature est stable (??)

Et les résultats uniquement avec l'image de fusion ???

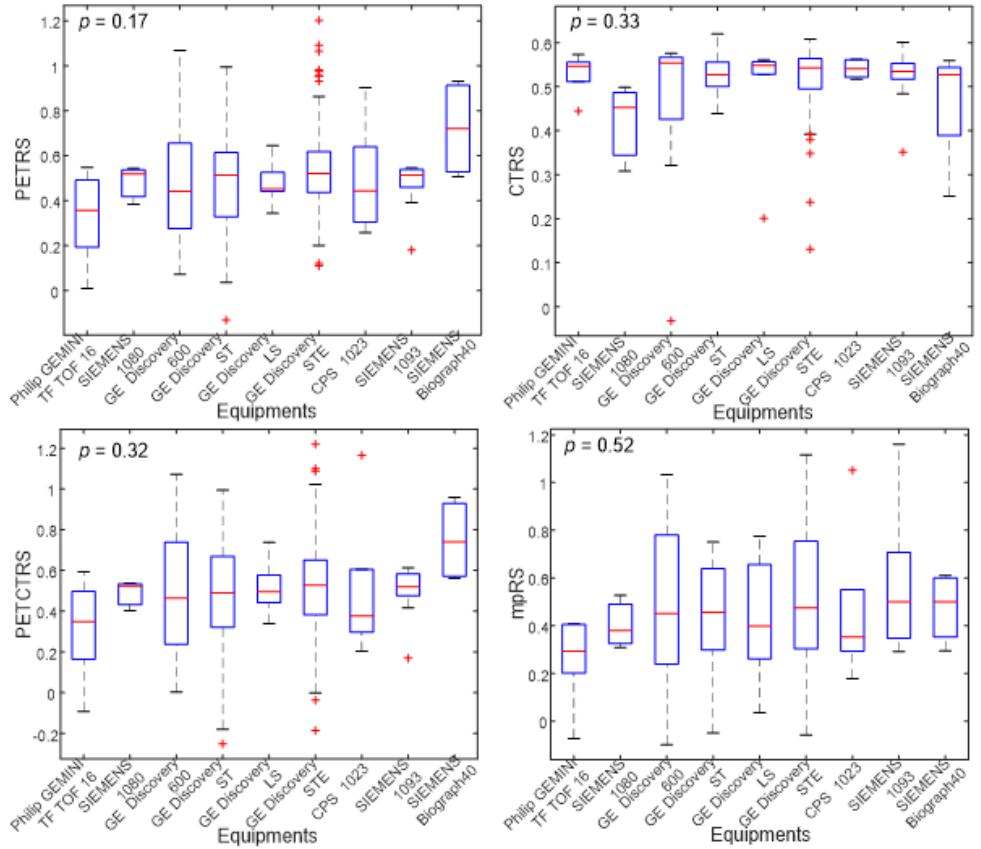

Fig S5. The distribution of PETRS, CTRS, PETCTRS and mpRS across the different acquisition equipment on the retrospective cohort. The p value in the left upper corner of each plot is the results of ANOVA analysis.

Signature mpRS

$$mpRS = (2-h)\begin{pmatrix} -0.58\times PET\_CMMean - 0.40\times PET\_SDim + 0.61\times PET\_SRLGE \\ -0.36\times PET\_Orientation - 0.61\times KLDiv\_mean \end{pmatrix} + 0.83h \quad (7.4)$$
$$+(h-1)(-1.91\times PET\_CHDensity - 1.25\times KLDiv\_CMEntropy + 0.93\times KLDiv\_SZE) + 0.32$$

ADC : h=1
SCC : h=2

PET_SDim ?

Orientation ???

CMMean means mean value of the calculated cooccurrence matix; DD means degree of diretion calculated from Texture spectrum matrix; Orientation means the main orientation of the ROI; SRLGE means short run low gray-level emphasis calculated from run length matrix; P1L2C2 means energy calculated from P1L2C2 layer; CMCS means cluster shade calculated from cooccurrence matix; CHDensity means convex hull area density; LRHGE means long run high gray-level emphasis calculated from run length matrix; L5E5L5 means energy calculated from L5E5L5 fillter image; S5R5E5 means energy calculated from S5R5E5 fillter image; P1L2C2 means energy calculated from P1L2C2 layer;Mean means mean value of the tumor region; CMentorpy means entorpy calculated from cooccurrence matix; SZE means short zone emphasis calculated from gray level size zone matrix.

Signature mpRS

$$mpRS = (2-h)\begin{pmatrix} -0.58\times PET\_CMMean - 0.40\times PET\_SDim + 0.61\times PET\_SRLGE \\ -0.36\times PET\_Orientation - 0.61\times KLDiv\_mean \end{pmatrix} + 0.83h \quad (7.4)$$
$$+(h-1)(-1.91\times PET\_CHDensity - 1.25\times KLDiv\_CMEntropy + 0.93\times KLDiv\_SZE) + 0.32$$

ADC : h=1
SCC : h=2

CMMean means mean value of the calculated cooccurrence matix; DD means degree of diretion calculated from Texture spectrum matrix; Orientation means the main orientation of the ROI; SRLGE means short run low gray-level emphasis calculated from run length matrix; P1L2C2 means energy calculated from P1L2C2 layer; CMCS means cluster shade calculated from cooccurrence matix; CHDensity means convex hull area density; LRHGE means long run high gray-level emphasis calculated from run length matrix; L5E5L5 means energy calculated from L5E5L5 fillter image; S5R5E5 means energy calculated from S5R5E5 fillter image; P1L2C2 means energy calculated from P1L2C2 layer;Mean means mean value of the tumor region; CMentorpy means entorpy calculated from cooccurrence matix; SZE means short zone emphasis calculated from gray level size zone matrix.

PET_SDim ?

Orientation ???

→ Pas d'index TDM dans la signature

Signature mpRS

$$mpRS = (2-h)\left(\begin{array}{l}-0.58\times PET\_CMMean - 0.40\times PET\_SDim + 0.61\times PET\_SRLGE \\ -0.36\times PET\_Orientation - 0.61\times KLDiv\_mean\end{array}\right) + 0.83h \quad (7.4)$$
$$+(h-1)\left(-1.91\times PET\_CHDensity - 1.25\times KLDiv\_CMEntropy + 0.93\times KLDiv\_SZE\right) + 0.32$$

ADC : h=1

SCC : h=2

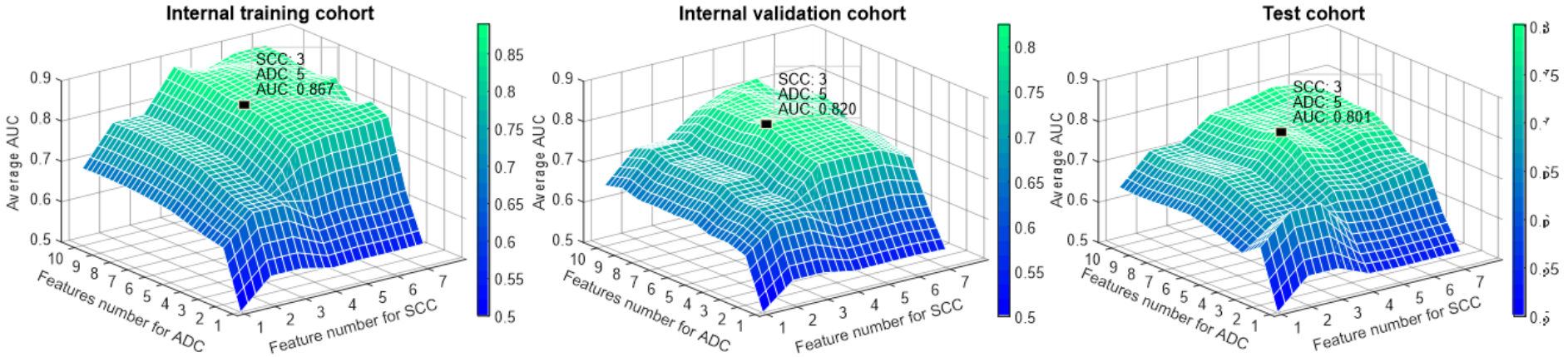

Fig S2. Average AUCs versus feature numbers of 5-fold cross validation (100 times) on internal training, internal validation, and test cohorts.

Signature mpRS

Fig. 4 Radiomics signatures of NSCLC patients. (a, b) The CT, PET, and fusion images for a patient with ADC NSCLC obtained 1 month before and 6 months after immunotherapy, which means the patient would have DCB since the start of immunotherapy and 6 months post-immunotherapy. (c, d) The CT, PET, and fusion images for a patient with ADC NSCLC obtained 1 month before and 9 months after immunotherapy, which means the patient would have DCB since the start of immunotherapy, but would have NDB after 9-month immunotherapy. The corresponding clinical feature and radiomics scores are shown in the bottom of each image

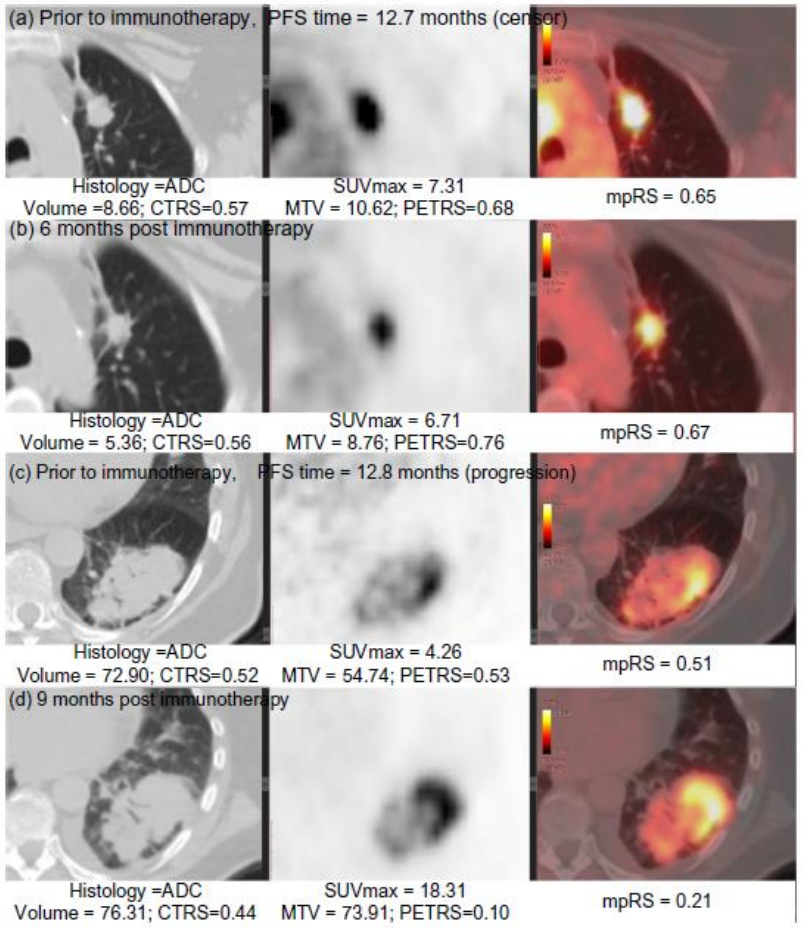

Signature mpRS → différence ADK/SCC

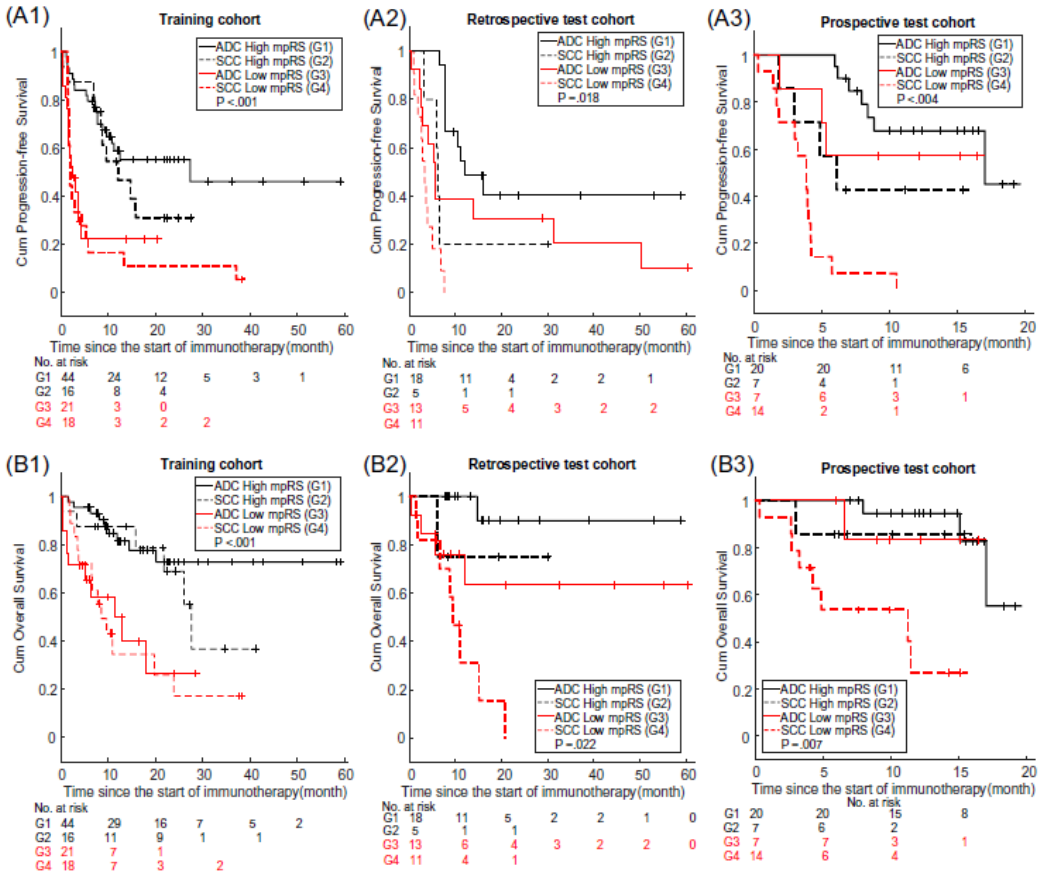

Fig. 6 Stratified Kaplan–Meier survival curves. (a–c) are stratified Kaplan–Meier survival curves of PFS according to mpRS on training, retrospective test and prospective test cohorts within the different subgroups of histology. (d–f) are stratified Kaplan-Meier survival curves of OS according to mpRS on training, retrospective test, and prospective test cohorts within the different subgroups of histology

→ Importance +++ de prendre en compte le sous-type histo

Nomogramme

DCB prediction nomogram

Univariable logistical regression analysis on the training cohort identified mpRS, distant metastasis, and ECOG status as strong predictors for response, and these were also validated in the test cohorts ($P < 0.05$, Supplemental Table S2). Through multivariable logistical regression analysis (Supplemental Table S3), ECOG scale and distant metastasis were predictive of a DCB response combined with the mpRS (Fig. 5a), and adding these clinical variables generated a higher AUC of 0.89, 0.86, and 0.86 in the training, retrospective test, and prospective test cohorts, respectively (Supplemental Table S1 and Fig. S4). This model was well calibrated in all three cohorts (Fig. 5c). The inclusion of ECOG scale and distant metastasis yielded a significant total NRI of 0.79 (95%CI 0.47–1.01, $P < 0.001$), 1.05 (95%CI 0.55–1.54, $P < .001$), and 1.20 (95%CI 0.75–1.65, $P < .001$) in the training, retrospective test, and prospective test cohorts, respectively.

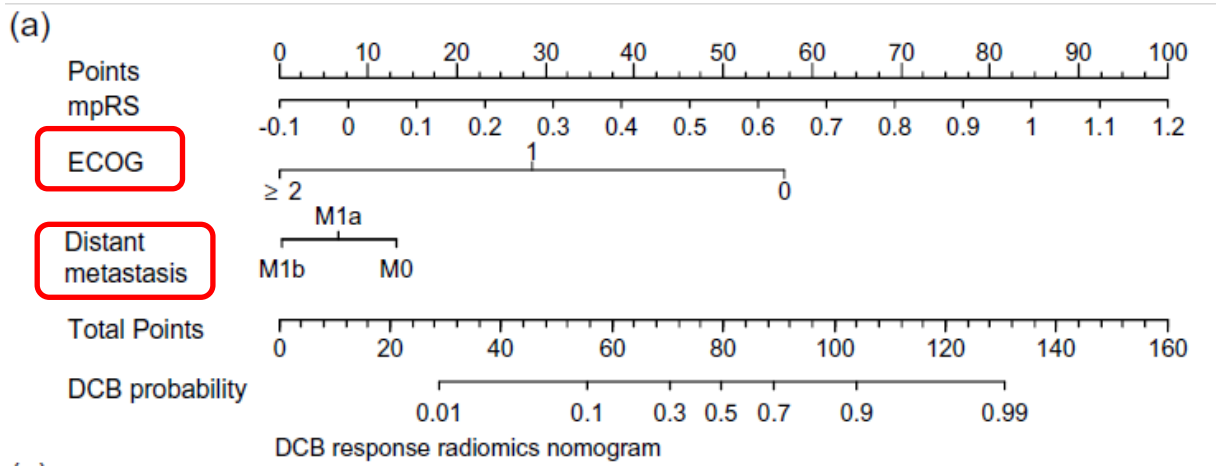

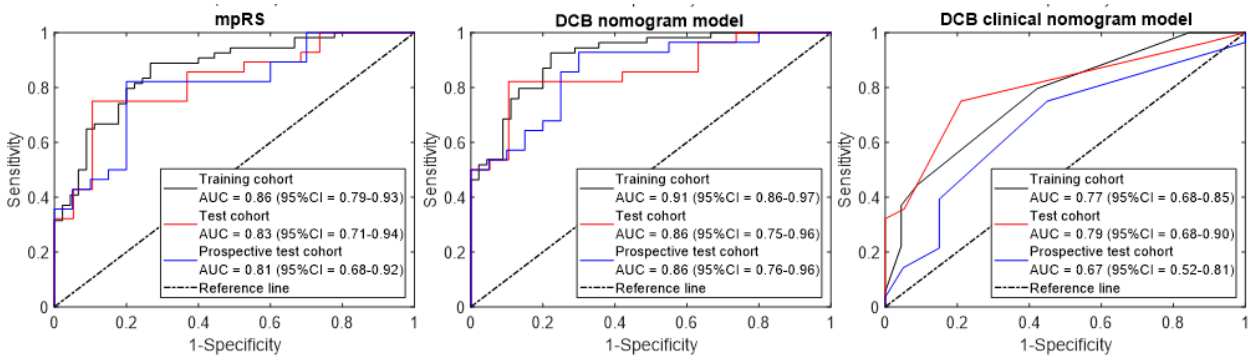

→ Amélioration des performances avec l'ajout de données cliniques

Statut ECOG

ECOG Performance Status

Developed by the Eastern Cooperative Oncology Group, Robert L. Comis, MD, Group Chair.*

GRADE	ECOG PERFORMANCE STATUS
0	Fully active, able to carry on all pre-disease performance without restriction
1	Restricted in physically strenuous activity but ambulatory and able to carry out work of a light or sedentary nature, e.g., light house work, office work
2	Ambulatory and capable of all selfcare but unable to carry out any work activities; up and about more than 50% of waking hours
3	Capable of only limited selfcare; confined to bed or chair more than 50% of waking hours
4	Completely disabled; cannot carry on any selfcare; totally confined to bed or chair
5	Dead

*Oken M, Creech R, Tormey D, et al. Toxicity and response criteria of the Eastern Cooperative Oncology Group. *Am J Clin Oncol.* 1982;5:649-655.

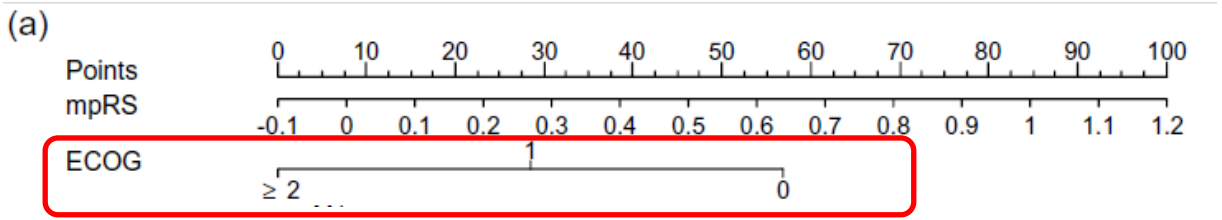

Prédiction PFS et OS

Table 2 Performance of different models in PFS and OS estimation

Category	Training cohort			Test cohort			Prospective cohort		
	C-index (95%CI)	AIC	*P*	C-index (95%CI)	AIC	*P*	C-index (95%CI)	AIC	*P*
PFS estimation									
mpRS	0.70 (0.64–0.76)	475.42	0.37§	0.67 (0.58-0.75)	231.03	0.81§	0.68 (0.59-0.78)	177.68	0.69§
PFS nomogram	0.74 (0.68–0.80)	464.21	0.12#	0.74 (0.66-0.82)	224.74	0.03#	0.77 (0.69-0.84)	175.02	0.051#
Clinical nomogram	0.66 (0.60–0.78)	479.93	0.006‡	0.68 (0.61-0.76)	226.61	0.01‡	0.66 (0.57-0.76)	186.46	0.027‡
OS estimation									
mpRS	0.74 (0.67–0.81)	291.99	0.92§	0.71 (0.56-0.85)	90.82	0.36§	0.76 (0.64-0.89)	78.46	0.38§
OS nomogram	0.83 (0.77–0.88)	266.82	< 0.001#	0.83 (0.71-0.94)	79.38	0.07#	0.80 (0.69-0.91)	78.62	0.55#
Clinical nomogram	0.74 (0.67–0.82)	286.77	< 0.001‡	0.79 (0.67-0.90)	79.40	0.16‡	0.67 (0.53-0.81)	87.00	.020‡

The C-index was compared between the mpRS and the mpRS nomogram

‡ The C-index was compared between the mpRS nomogram and clinical nomogram

§ The C-index was compared between the mpRS and clinical nomogram

→ Le nomogramme permet aussi de prédire la PFS et l'OS

Etude pilote : suivi de l'évolution

Pilot study for longitudinal assessment of the radiomics signature

A further analysis using subsequent follow-up scans, when available, showed the mpRS generated from the follow-up PET/CT images during treatment could also predict follow-up DCB with an AUC of 0.82 (95%CI 0.63–1.00). Further, it had a decreasing trend with time (Supplemental Fig. S7), suggesting that the risk of progression increased with time.

→ La signature reste prédictive au cours du suivi

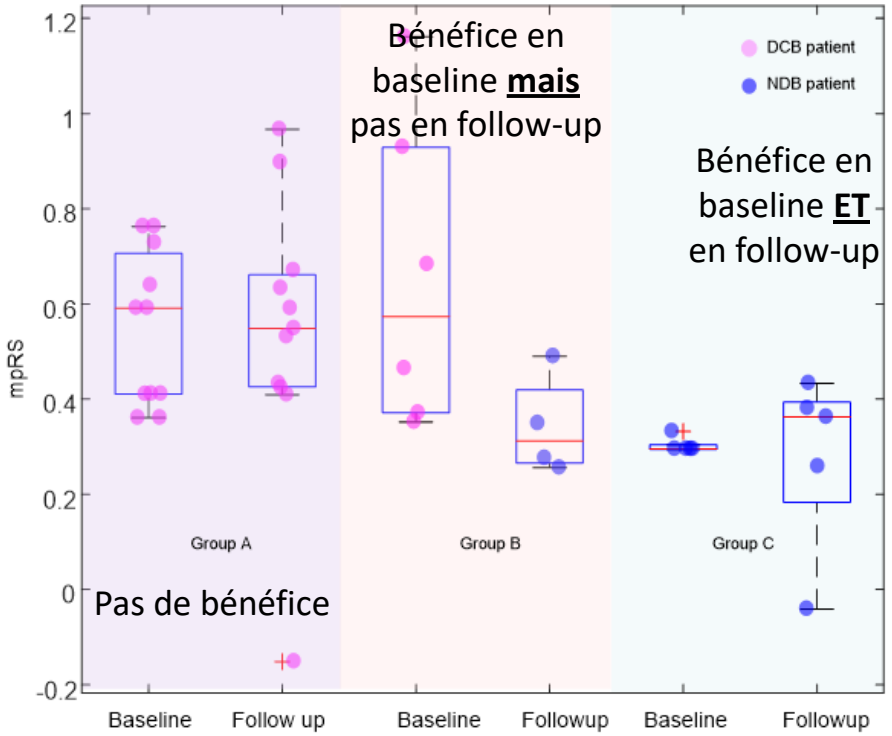

Fig S7. The multiparametric radiomics signature at different time points of different groups of patients. Group A means patients with NDB for anti-PD-1/PD-L1 immunotherapy at baseline; Group means patients who have DCB for anti-PD-1/PD-L1 immunotherapy at baseline time point but NDB at follow up time point (progressed within 6 months since the follow-up scan time); Group C means patients with DCB for anti-PD-1/PD-L1 immunotherapy at both baseline and follow up time points (progression-free survival time longer than 6 months since the follow-up scan time).

Conclusion

Des résultats encourageants mais il reste des zones d'ombre :

- Impact des protocoles d'acquisition
- Pouvoir prédictif des images de fusion uniquement
- Décryptage des index de la signature

Peut-on essayer de reproduire ces résultats ? → thèse de médecine de Pierre-Adrien Vion